Quantized Constant Envelope Precoding With PSK and QAM Signaling

Hela Jedda, *Student Member, IEEE*, Amine Mezghani, *Member, IEEE*, A. Lee Swindlehurst, *Fellow, IEEE*, and Josef A. Nossek, *Life Fellow, IEEE*

***Abstract*— Coarsely quantized massive multiple-input multiple-output (MIMO) systems are gaining more interest due to their power efficiency. We present a new precoding technique to mitigate the multi-user interference and the quantization distortions in a downlink multi-user MIMO system with coarsely quantized constant envelope (QCE) signals at the transmitter. The transmit signal vector is optimized for every desired received vector taking into account a relaxed version of the QCE constraint. The optimization is based on maximizing the safety margin to the decision thresholds of the receiver constellation modulation. Due to the linear property of the objective function and the constraints, the optimization problem is formulated as a linear programming problem. The simulation results show a significant gain in terms of the uncoded bit error rate compared to the existing precoding techniques.**

***Index Terms*— Constant envelope, coarse quantization, constructive interference, downlink massive multi-user MIMO, precoding.**

I. Introduction

THE next generation of mobile communication aims at increasing 1000-fold the network capacity, 10-100-fold the number of connected devices and decreasing 5-fold the latency time and the power consumption compared to 4G networks [1]. To achieve these challenging requirements, the following technologies are the subject of current research:

- massive Multiple-Input Multiple-Output (MIMO) systems, where the Base Stations (BSs) are equipped with a very large number of antennas (100 or more) that can simultaneously serve many users [2]–[6],
- millimeter-Wave (mmW) communication, i.e. frequencies ranging between 30 GHz and 300 GHz, where the spectrum is less crowded and greater bandwidth is available [7]–[9] and
- smaller cells with ranges on the order of 10-200 m, i.e. pico- and femtocells.

First, massive MIMO systems lead to a drastic increase in the number of Radio Frequency (RF) chains at the BS and hence in the number of the wireless front-end hardware components. Second, mmW communication implies that the wireless front-end hardware components are operated at much higher frequencies. Third, reducing the cell size means that the number of cells per unit area is increased and thus results in a much more dense wireless network. Combining the three technologies means a dramatic increase in the number of RF hardware elements operating at very high frequencies per unit area. Hence, the RF power consumption per unit area alarmingly increases. While the above technologies are foreseen as key technologies for future communication systems, the increase in power consumption represents a crucial concern.

The most critical front-end elements in terms of power consumption, depending on whether the large number of antennas is situated at the receiver or at the transmitter, are the Analog-to-Digital Converters (ADCs) in the uplink scenario, and mainly the Power Amplifiers (PAs) and secondarily the Digital-to-Analog Converters (DACs) in the downlink scenario, which is the focus of this contribution. According to [10] and [11], the PA is considered as the most power hungry device at the transmitter side. When the PA is run in the saturation region, i.e. the highly non-linear region, high power efficiency is achieved and hence less power is consumed [12]. However, the saturation region implies strong non-linear signal distortions. To omit the signal distortions, while keeping the PA operate in the saturation region, the input signals should fulfill the Constant Envelope (CE) property, which leads to a unit Peak-to-Average-Power Ratio (PAPR).

To this end, polar (phase-based) DACs at the transmitter are designed to convert the discrete-time and discrete-value base-band signals into continuous-time but discrete-value, i.e. discrete-phase, CE signals. The number of possible discrete phases is determined by the resolution of the DAC. The larger the resolution is, the more accurate the phase information at the DAC's output is, but the larger its power consumption is [13]. To further reduce the hardware power consumption,

Manuscript received January 30, 2018; revised September 9, 2018; accepted September 9, 2018. Date of publication October 9, 2018; date of current version December 10, 2018. This work was supported in part by the National Science Foundation under Grants ECCS-1547155 and CCF-1703635 and in part by the Hans Fischer Senior Fellowship from the Technical University of Munich Institute for Advanced Study. The associate editor coordinating the review of this paper and approving it for publication was X. Yuan. *(Corresponding author: Hela Jedda.)*

H. Jedda is with the Associate Professorship of Signal Processing, Technical University of Munich, 80290 Munich, Germany (e-mail: hela.jedda@tum.de).

A. Mezghani is with the Wireless Networking and Communications Group, The University of Texas at Austin, Austin, TX 78712 USA (e-mail: amine.mezghani@utexas.edu).

A. L. Swindlehurst is with the Center for Pervasive Communications and Computing, University of California at Irvine, Irvine, CA 92697 USA (e-mail: swindle@uci.edu).

J. A. Nossek is with the Associate Professorship of Signal Processing, Technical University of Munich, 80290 Munich, Germany, and also with the Department of Teleinformatics Engineering, Federal University of Ceará, Fortaleza 60020-181, Brazil (e-mail: josef.a.nossek@tum.de).

Color versions of one or more of the figures in this paper are available online at http://ieeexplore.ieee.org.

Digital Object Identifier 10.1109/TWC.2018.2873386

the DAC's resolution can be reduced. The use of coarsely quantized DACs is also beneficial in terms of reduced cost and circuit area and can further simplify the surrounding RF circuitry due to the relaxed linearity constraint, leading to very efficient hardware implementations. In this way, the power consumption is reduced twofold: power efficient PAs due to the CE signals and less power consuming polar DACs due to the low resolution. However, this approach can lead to non-linear distortions that degrade the system performance and have to be mitigated by the precoder design in massive Multi-User (MU) MIMO downlink systems.

A. Related Works

Many works have addressed the precoding problem in the context of CE transmit signals for massive MIMO systems such that [14]–[18], where the Multi-User Interference (MUI) is minimized subject to the CE constraint. Another work [19] opts for minimizing an upper bound of the Symbol Error Rate (SER) in the case of single-user Multiple-Input Single-Output (MISO) systems for two strategies: antenna-subset selection, where a subset of the antennas is selected for transmission, and unequal power allocation among the antennas, where the magnitude of the transmit signal at each antenna is kept constant over a transmission period but the signal magnitudes at distinct transmit antennas are not necessarily equal. The authors of [20] jointly optimize the transmit CE precoding and the constellation in order to minimize the SER in a MISO multicast system. Recent works in [21] and [22] exploit the constructive part of the MUI to design the CE precoder. The authors in [23] design a CE precoder to maximize the Signal-to-Leakage-plus-Noise Ratio (SLNR). In [24], a CE precoder is jointly designed with the receive beamforming to minimize the SER for point-to-point MIMO systems, while adopting antenna grouping for multi-stream transmission. In the above contributions, the DACs are assumed to have infinite resolution.

The contribution in [25] is an early work that addressed the precoding task with low resolution DACs at the transmitter. A linear Minimum Mean Squared Error (MMSE) precoder is designed, while quantization distortion is taken into account. This precoding design is not given in the context of coarsely Quantized Constant Envelope (QCE) signals since the DACs are not polar but Cartesian (in-phase- and quadrature). However, the extreme case of 1-bit DACs in [25] represents a special case of coarsely QCE signals. Many contributions in the literature have studied this special case. They can be categorized in two groups: linear and non-linear precoders. In addition to the linear precoder in [25], we introduced in [26] another linear precoder, where the second-order statistics of the 1-bit DAC signals are computed based on Price's theorem [27]. Non-linear precoding techniques in this context were introduced in [28]–[33]. The non-linear methods can be classified with respect to two design criteria: symbol-wise Minimum Squared Error (MSE) and symbol-wise Maximum Safety Margin (MSM) exploiting the idea of constructive interference. In the context of symbol-wise MSE, the authors in [29] presented a convex formulation of the problem and applied it to higher-order modulations [30]. The problem formulation is based on semidefinite relaxation and squared ℓ_∞-norm relaxation. The same optimization problem was solved more efficiently in [32] and [34].

In the context of symbol-wise MSM in [28], we presented a precoding technique based on a minimum Bit Error Rate (BER) criterion and made use of the box norm (ℓ_∞) to relax the 1-bit constraint. Recently, the work in [33] proposed a method to significantly improve linear precoding solutions in conjunction with 1-bit quantization by properly perturbing the linearly precoded signal for each given input signal to favorably impact the probability of correct detection. In [31] the safety margin to the decision thresholds of the received Phase-Shift Keying (PSK) symbols is maximized subject to a relaxed 1-bit constraint using linear programming for flat-fading channels and extended in [35] for frequency-selective channels. The same optimization problem was solved by the Branch-and Bound algorithm in [36] for the special case of 4-PSK.

To the best of our knowledge, the only works that have considered the case of coarsely QCE transmit signals are [37]–[40]. In [37], we propose a symbol-wise MSE precoder based on gradient-descent under a strict CE constraint or a relaxed polygon constraint. In [38], the authors extend the method in [29] to fit the context of QCE transmit signals. In [39], the authors use a greedy approach for the precoder design while using symbol-wise MSE as the design criterion. The contribution in [40] addresses the task of QCE precoding in the context of using a single common PA and separate digital phase shifters for the antenna front-ends. The optimization problem consists of designing the QCE precoder while minimizing the MUI, and the idea of constructive interference, [41], [42], is not exploited as in our work. The concept of QCE precoding and general constellations for flat-fading channels is studied in this contribution and is extended partially to frequency-selective channels in [35] and [43]. It is worth mentioning that the QCE precoding can be combined with appropriate pulse shaping strategies as in [44] and [45] to ensure an efficient spectral confinement. In [46], it was shown that CE precoding is still power efficient even when considering time-based processing. The same investigation can be conducted for the case of QCE precoding. Here, we focus rather on the spatial design problem.

B. Main Contributions

The main contributions in this paper are summarized as follows

1) We propose a method for QCE precoding in the context of massive MIMO systems, where the transmit signals have constant magnitude and phases drawn from a discrete set. The precoder design is based on maximizing the safety margin to the decision thresholds while exploiting the idea of constructive interference. The design criterion in [31] is extended to the coarse QCE case, where the QCE constraint is relaxed to a polygon constraint to ensure convexity. While the proposed design for PSK signaling is similar to the work

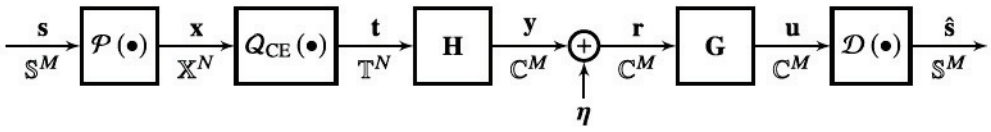

Fig. 1. Downlink MU-MIMO system model.

in [22], we employ a relaxed polygon constraint rather than a relaxed unit circle constraint as in [22]. Since the polygon constraint can be expressed in terms of linear convex inequalities, this allows us to solve the problem using linear programming techniques, which are significantly more efficient. The simulation results related to the proposed method show a significant gain in terms of the uncoded BER compared to the method in [22].

2) We extend the proposed QCE precoder to the case of Quadrature Amplitude Modulation (QAM) signaling. The constructive interference idea has been applied previously to QAM signals in [47]–[49] for different design criteria and in other contexts, e.g for power minimization. In this contribution, we describe the constructive interference regions with modified mathematical expressions and a general QAM constellation that include the safety margin to fit our design criterion. We solve the formulated problem within a pure linear programming framework, one of the most studied problems in optimization. We also provided results where the receiver blindly estimates the QAM scaling factor. We extend the proposed QCE precoder to the case of QAM signaling.

C. Remainder and Notation

The remainder of this paper is organized as follows. In Section II, we present the system model. In Section III, the motivation behind formulating the precoding problem as a linear programming problem is explained. Sections IV and V present the corresponding optimization problems for PSK and QAM signals, respectively. The complexity of each optimization problem is discussed in Section VI. Simulation results are introduced in VII. Finally, Section VIII summarizes this work.

Notation: Bold lower case and upper case letters indicate vectors and matrices, non-bold letters express scalars. The operators $(.)^*$, $(.)^{\mathrm{T}}$ and $(.)^{\mathrm{H}}$ stand for complex conjugation, transposition and Hermitian transposition, respectively. The $n \times n$ identity (zero) matrix is denoted by $\mathbf{I}_n$ ($\mathbf{0}_{n,n}$). The n dimensional one (zero) vector is denoted by $\mathbf{1}_n$ ($\mathbf{0}_n$). The vector $\mathbf{e}_m$ represents a zero-vector with 1 at the m-th position. Additionally, $\mathrm{diag}\,(\mathbf{a})$ denotes a diagonal matrix containing the entries of the vector $\mathbf{a}$. Every vector $\mathbf{a}$ of dimension L is defined as $\mathbf{a} = \sum_{\ell=1}^{L} a_\ell \mathbf{e}_l$. The operator $\otimes$ denotes the Kronecker product. The operator $\leq$ in the context of vector inequalities applies element-wise to the vector entries.

II. System Model

The system model shown in Fig.1 consists of a single-cell massive MU-MIMO downlink scenario with coarsely QCE signals at the transmitter. The BS is equipped with N antennas and serves M single-antenna users simultaneously, where $N \gg M$. The input signal vector $\mathbf{s}$ contains the signals to be transmitted to each of the M users. Each user's signal is drawn from the set $\mathbb{S}$ that represents either an S-PSK or S-QAM constellation, where S denotes the number of constellation points. We assume that $\mathrm{E}[\mathbf{s}] = \mathbf{0}_M$ and $\mathrm{E}[\mathbf{s}\mathbf{s}^{\mathrm{H}}] = \sigma_{\mathrm{s}}^2 \mathbf{I}_M$. The signal vector $\mathbf{s}$ is precoded into the vector $\mathbf{x} \in \mathbb{X}^N$ prior to the DACs. The entries of $\mathbf{x}$ are amplitude-constrained and the set $\mathbb{X}$ is a convex set that can be described by linear inequalities as explained in Section III-A. The non-linear function $\mathcal{P}(\bullet)$ is a symbol-wise precoder designed to reduce the distortions caused by the coarse quantization and the MUI. The operator $\mathcal{Q}_{\text{CE}}(\bullet)$ models the non-linear behavior of the low-resolution polar DACs combined with the power allocation at the PAs as

$$\mathbf{t} = \mathcal{Q}_{\text{CE}}(\mathbf{x}) = \sqrt{\frac{P_{\text{tx}}}{N}}\, \mathrm{e}^{\mathrm{j}\, \mathcal{Q}_\phi(\arg(\mathbf{x}))}, \tag{1}$$

where the total transmit power P_{tx} is allocated equally among the transmit antennas. The phase quantizer $\mathcal{Q}_\phi(\bullet)$ is a symmetric uniform real-valued quantizer. It is characterized by its resolution q that defines the number of discrete output phases

$$Q = 2^q. \tag{2}$$

In other words, the 2π-phase range is divided into Q $\frac{2\pi}{Q}$-rotationally symmetric sectors. The input signal that belongs to the k-th sector is quantized (mapped) to $\mathrm{e}^{\mathrm{j}(2k-1)\frac{\pi}{Q}}$. This can be mathematically expressed as

$$\mathcal{Q}_\phi(\arg(x_n)) = \left(\left\lfloor \frac{\arg(x_n)}{2\pi/Q} \right\rfloor + \frac{1}{2} \right) \frac{2\pi}{Q}, \quad n = 1, \cdots, N. \tag{3}$$

Thus, the information after the CE quantizer lies only in the phase. Hence, the set $\mathbb{T}$ is defined as

$$\mathbb{T} = \left\{ \sqrt{\frac{P_{\text{tx}}}{N}} \exp\left(\mathrm{j}\,(2i-1)\,\frac{\pi}{Q} \right) : i = 1, \cdots, Q \right\}. \tag{4}$$

Note that directly designing the mapping between $\mathbf{s}$ and $\mathbf{t}$ would lead to a discrete optimization problem that is NP-hard. Thus, we design in an intermediate step the vector $\mathbf{x} \in \mathbb{X}^N$, where $\mathbb{X}$ represents a convex relaxation of $\mathbb{T}$ as explained in Section III-A.

The signal $\mathbf{t}$ is transmitted through a flat-fading channel that is modeled by the matrix $\mathbf{H}$ of elements h_{mn}, $m = 1, \cdots, M$, $n = 1, \cdots, N$. At the M receive antennas, Additive White Gaussian Noise (AWGN), which is denoted by the vector $\boldsymbol{\eta} \sim \mathcal{CN}_{\mathbb{C}}\,(\mathbf{0}_M, \mathbf{C}_{\boldsymbol{\eta}} = \mathbf{I}_M)$, perturbs the received signals

$$\mathbf{r} = \mathbf{H}\mathbf{t} + \boldsymbol{\eta}. \tag{5}$$

Since the precoder is implemented symbol-by-symbol, joint processing at the receiver would require not only knowledge of the channel but also the desired received signals themselves, which are unknown at the receiver. Therefore, the precoder is designed such that, without any noise, the received signals would lie in their intended decision regions and no joint receive processing is necessary. Additionally, coherent data transmission with multiple BS antennas leads to an antenna gain, which depends on the channel realization. Hence, the precoder design leads in the best case scenario to the fact that, the entries of the received signal vector $\mathbf{r}$ do not belong to the nominal decision regions of $\mathbb{S}$ but to a scaled version of them. Therefore, rescaling the received signal at each receive antenna is required to ensure that the received signal belongs to the nominal decision region. The rescaling operation is modeled by the diagonal real-valued matrix $\mathbf{G}$, as follows

$$\mathbf{u} = \mathbf{G}\left(\mathbf{H}\mathbf{t} + \boldsymbol{\eta}\right), \tag{6}$$

where

$$\mathbf{G} = \sum_{m=1}^{M} g_m \mathbf{e}_m \mathbf{e}_m^{\mathrm{T}}, \tag{7}$$

with $g_m > 0,\ m = 0, \cdots, M$. The coefficients g_m are blindly estimated at the receiver over a block of received symbols as explained in Section V-F. Note that no receive processing $\mathbf{G}$ is required if $\mathbb{S}$ represents the PSK constellation. Finally, based on the decision regions to which the entries of the signal $\mathbf{u}$ belong, the decision operation $\mathcal{D}(\bullet)$ produces the detected symbols $\hat{\mathbf{s}}$ at the users

$$\hat{\mathbf{s}} = \mathcal{D}\left(\mathbf{G}\left(\mathbf{H}\mathbf{t} + \boldsymbol{\eta}\right)\right). \tag{8}$$

III. Precoding Task

In this work, we make use of the idea of constructive interference optimization [41], [42]. When the downlink channel and all users' data are known at the transmitter, instantaneous constructive MUI can be exploited to move the received signals further from the decision thresholds [42]. In contrast to this, conventional precoding methods (MMSE, Zero-forcing) aim at minimizing the total MUI such that the received signals lie as close as possible to the nominal constellation points. Constructive interference optimization exploits the larger symbol decision regions and thus leads to a more relaxed optimization.

For every given input signal $\mathbf{s}$ and for each channel realization $\mathbf{H}$, the precoding task is to find

$$\mathbf{x} = \mathcal{P}\left(\mathbf{s}, \mathbf{H}\right). \tag{9}$$

The task consists of designing the transmit vector $\mathbf{x}$ such that $\hat{\mathbf{s}} = \mathbf{s}$ holds true with high probability to reduce the detection error probability. The symbol-wise precoder aims to mitigate all sources of distortion:

- the quantization distortions
- the channel distortions, and
- the AWGN.

Our goal is to develop a problem formulation that jointly minimizes all three distortion sources.

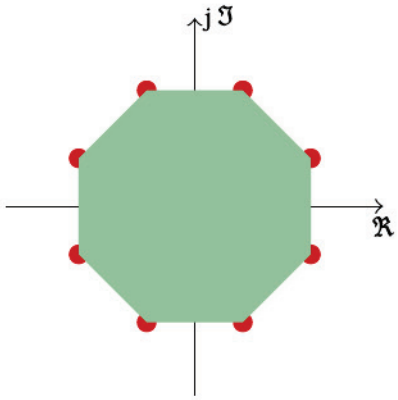

Fig. 2. Illustration of the relaxed polygon constraint for $Q = 8$.

A. Mitigation of the Quantization Distortions

First, it is obvious that the quantization distortions can be omitted if we design the precoded vector $\mathbf{x}$ such that

$$\mathbf{x} \in \mathbb{T}^N, \tag{10}$$

i.e. $\mathbb{X} = \mathbb{T}$. This would ensure that the quantizer $\mathcal{Q}_{\mathrm{CE}}(\bullet)$ produces no distortion, and we would have an undistorted transmit signal $\mathbf{t} = \mathbf{x}$. However, the QCE constraint in (10) would lead to a discrete optimization problem due to the discrete nature of the set $\mathbb{T}$. To avoid this problem, we relax the discrete set $\mathbb{T}$ to the convex set $\mathbb{X}$ that represents the polygon built by the Q scaled PSK points of the set $\mathbb{T}$. Thus, the QCE constraint is relaxed to a convex constraint that we call the relaxed polygon constraint. Fig. 2 illustrates the relaxed polygon constraint for the case of $Q = 8$. Instead of designing $\mathbf{x} \in \mathbb{T}^N$ to completely eliminate the quantization distortions, we design $\mathbf{x} \in \mathbb{X}^N$ to minimize them.

The set $\mathbb{X}$ can be mathematically described by a set of linear inequalities. For q-bit polar DACs, i.e., where the transmitted data are constrained to be Q scaled PSK symbols, the polygon can be constructed by the intersection of $Q/4$ squares that have an angular shift of $2\pi/Q$. To this end, we define the rotation matrix $\mathbf{R}_i$ of angle $\beta_i = \frac{2\pi}{Q}(i-1)$ as

$$\mathbf{R}_i = \begin{bmatrix} \cos\beta_i & \sin\beta_i \\ -\sin\beta_i & \cos\beta_i \end{bmatrix} \otimes \mathbf{I}_N, \quad i = 1, \ldots, Q/4. \tag{11}$$

The system of inequalities that considers the feasible set, i.e. the relaxed polygon constraint, and hence relaxes the constraint in (10) is given by

$$\begin{bmatrix} \mathbf{R}_1^{\mathrm{T}} & -\mathbf{R}_1^{\mathrm{T}} & \cdots & \mathbf{R}_{\frac{Q}{4}}^{\mathrm{T}} & -\mathbf{R}_{\frac{Q}{4}}^{\mathrm{T}} \end{bmatrix}^{\mathrm{T}} \bar{\mathbf{x}} \leq \sqrt{\frac{P_{\mathrm{tx}}}{N}} \cos\left(\frac{\pi}{Q}\right) \mathbf{1}_{NQ}, \tag{12}$$

where $\bar{\mathbf{x}} = \begin{bmatrix} \Re\{\mathbf{x}\}^{\mathrm{T}} & \Im\{\mathbf{x}\}^{\mathrm{T}} \end{bmatrix}^{\mathrm{T}}$. Since $\mathbf{R}_1 = \mathbf{I}_{2N}$, the first $4N$ inequalities in (12) define the bounds for $\bar{\mathbf{x}}$. Hence, the relaxed polygon constraint, i.e. $\mathbf{x} \in \mathbb{X}^N$, is equivalent to

$$-\sqrt{\frac{P_{\mathrm{tx}}}{2N}} \cos\left(\frac{\pi}{Q}\right) \mathbf{1}_{2N} \leq \bar{\mathbf{x}} \leq \sqrt{\frac{P_{\mathrm{tx}}}{N}} \cos\left(\frac{\pi}{Q}\right) \mathbf{1}_{2N},$$

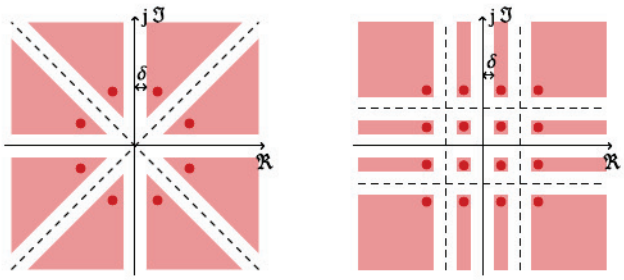

(a) 8-PSK. (b) 16-QAM.

Fig. 3. Decision and symbol regions (in red).

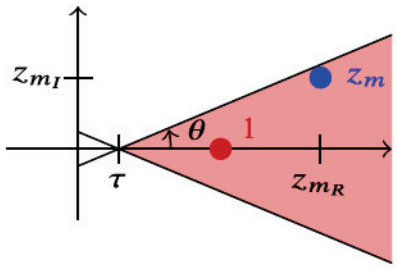

Fig. 4. Illustration of the PSK symbol region in a modified coordinate system.

and

$$\underbrace{\begin{bmatrix}\mathbf{R}_2^{\mathrm{T}} & -\mathbf{R}_2^{\mathrm{T}} & \cdots & \mathbf{R}_{\frac{Q}{4}}^{\mathrm{T}} & -\mathbf{R}_{\frac{Q}{4}}^{\mathrm{T}}\end{bmatrix}^{\mathrm{T}}}_{=\mathbf{E}} \bar{\mathbf{x}} \leq \sqrt{\frac{P_{\mathrm{tx}}}{N}} \cos\left(\frac{\pi}{Q}\right) \mathbf{1}_{N(Q-4)}. \tag{13}$$

This reformulation leads to significant computational savings since the final optimization problem will be written as a linear program with bounded variables. As discussed in Section VI, it is beneficial in terms of computational complexity to have fewer inequalities.

B. Counteracting the Channel Distortions and the Noise

Second, to minimize the channel distortions and the noise, we look deeper into the properties of the constellations. As illustrated in Fig. 3a and Fig. 3b, each constellation is defined by thresholds that separate the distinct decision regions of the constellation points. In total, we have as many contiguous decision regions as constellation points. Each constellation symbol lies within a Symbol Region (SR) that is a downscaled version of the decision region. In contrast to the decision region, the SR has a safety margin denoted by δ that separates it from the decision thresholds. When each entry of the noiseless received signal vector $\mathbf{y}$ belongs to the correct SR and thus the correct decision region, the channel distortions are mitigated. Additionally, the safety margin δ has to be large enough such that, when perturbed by the additive noise, the received signals do not jump to unintended neighboring decision regions.

C. General Problem Formulation

In summary, the problem formulation has to take into account the relaxed QCE constraint in (13), the SR for each received signal and maximizing the safety margin. Thus, the optimization problem for the symbol-wise precoder, which we call the MSM precoder, can be written in general as follows

$$\max_{\mathbf{x}} \delta \tag{14}$$

$$\text{s.t.} \quad y'_m \in \mathrm{SR}_m, \quad \forall m \tag{15}$$

$$\text{and } \mathbf{x} \in \mathbb{X}^N, \tag{16}$$

where

$$\mathbf{y}' = \mathbf{H}\mathbf{x} \tag{17}$$

represents the relaxation of $\mathbf{y}$ due to the relaxation of (10) to (13). Exact expressions for the safety margin δ and the SRs as a function of $\mathbf{x}$ are provided in Section IV and Section V for PSK and QAM signaling, respectively.

IV. Problem Formulation for PSK Signaling

A. Symbol Region for PSK Signals

In this section, we assume that the input signals s_m, $m = 1, \cdots, M$, belong to the S-PSK constellation. The set $\mathbb{S}$ in this case is defined as

$$\mathbb{S} := \{\exp(\mathrm{j}(2i-1)\theta) : i = 1, \cdots, S\}, \text{ where } \theta = \frac{\pi}{S}. \tag{18}$$

Each SR in the PSK constellation, as shown in Fig. 3a, is a circular sector of infinite radius and angle 2θ. To find mathematical expressions for the SRs, the original coordinate system is rotated by the phase of the symbol of interest s_m to get a modified coordinate system as illustrated in Fig. 4. The coordinates of the noiseless received signal y'_m in the modified coordinate system are given by

$$z_{m_R} = \Re\{y'_m s_m^*\} \frac{1}{|s_m|} \tag{19}$$

$$z_{m_I} = \Im\{y'_m s_m^*\} \frac{1}{|s_m|}. \tag{20}$$

Since PSK signals have unit magnitude, plugging (17) into the above equations gives

$$z_{m_R} = \Re\{\mathbf{e}_m^{\mathrm{T}} \mathbf{H}\mathbf{x} s_m^*\} = \Re\{\mathbf{e}_m^{\mathrm{T}} \tilde{\mathbf{H}}\mathbf{x}\} \tag{21}$$

$$z_{m_I} = \Im\{\mathbf{e}_m^{\mathrm{T}} \mathbf{H}\mathbf{x} s_m^*\} = \Im\{\mathbf{e}_m^{\mathrm{T}} \tilde{\mathbf{H}}\mathbf{x}\}, \tag{22}$$

where

$$\tilde{\mathbf{H}} = \mathrm{diag}(\mathbf{s}^*)\mathbf{H}. \tag{23}$$

The m-th SR can be hence described by

$$z_{m_R} \geq \tau \tag{24}$$

$$|z_{m_I}| \leq (z_{m_R} - \tau)\tan\theta, \quad \forall m, \tag{25}$$

where $\tau = \frac{\delta}{\sin\theta}$. Note that the inequality in (24) is already fulfilled if the inequality in (25) is satisfied. Plugging (21) and (22) into (25), the SRs for all M users can be defined by

$$|\Im\{\tilde{\mathbf{H}}\mathbf{x}\}| \leq \left(\Re\{\tilde{\mathbf{H}}\mathbf{x}\} - \tau \mathbf{1}_M\right)\tan\theta \tag{26}$$

as also given in [42]. When using the following real-valued representation

$$\Re\{\tilde{\mathbf{H}}\mathbf{x}\} = \underbrace{\begin{bmatrix}\Re\{\tilde{\mathbf{H}}\} & -\Im\{\tilde{\mathbf{H}}\}\end{bmatrix}}_{=\mathbf{A}} \begin{bmatrix}\Re\{\mathbf{x}\}\\ \Im\{\mathbf{x}\}\end{bmatrix} = \mathbf{A}\bar{\mathbf{x}} \quad (27)$$

$$\Im\{\tilde{\mathbf{H}}\mathbf{x}\} = \underbrace{\begin{bmatrix}\Im\{\tilde{\mathbf{H}}\} & \Re\{\tilde{\mathbf{H}}\}\end{bmatrix}}_{=\mathbf{B}} \begin{bmatrix}\Re\{\mathbf{x}\}\\ \Im\{\mathbf{x}\}\end{bmatrix} = \mathbf{B}\bar{\mathbf{x}}, \quad (28)$$

the SR constraints in (15) can be rewritten as

$$\begin{bmatrix}\mathbf{B} - \tan\theta\mathbf{A} & \frac{1}{\cos\theta}\mathbf{1}_M\\ -\mathbf{B} - \tan\theta\mathbf{A} & \frac{1}{\cos\theta}\mathbf{1}_M\end{bmatrix}\begin{bmatrix}\bar{\mathbf{x}}\\ \delta\end{bmatrix} \leq \mathbf{0}_{2M}. \quad (29)$$

B. Safety Margin for PSK Signals

The safety margin δ in (14) can be expressed for the PSK case as

$$\delta = \min_m \left(\sin(\theta)\mathbf{z}_R - \cos(\theta)\left|\mathbf{z}_I\right|\right), \quad (30)$$

where the operator $|\bullet|$ is applied element-wise to the entries of $\mathbf{z}_\mathrm{I}$. Note that an equivalent objective function was introduced in [22] in the context of continuous-phase CE precoding for PSK signaling. In [22], the strict CE constraint is relaxed to the convex unit circle, whereas in our work the QCE constraint is relaxed to the linear polygon constraint. Consequently, due to the linear objective function and the linear constraints, our optimization problem can be formulated as a linear programming problem unlike [22].

C. Optimization Problem

Finally, the optimization problem for the symbol-wise precoder with PSK signaling is obtained by combining (14), (29) and (13) and is expressed for the case of $P_\mathrm{tx} = N$ as

$$\begin{aligned}&\max_{\bar{\mathbf{x}},\delta} \quad \begin{bmatrix}\mathbf{0}_{2N}^\mathrm{T} & 1\end{bmatrix}\begin{bmatrix}\bar{\mathbf{x}}\\ \delta\end{bmatrix}\\ &\text{s.t.} \quad \begin{bmatrix}\mathbf{B} - \tan\theta\mathbf{A} & \frac{1}{\cos\theta}\mathbf{1}_M\\ -\mathbf{B} - \tan\theta\mathbf{A} & \frac{1}{\cos\theta}\mathbf{1}_M\\ \mathbf{E} & \mathbf{0}_{N(Q-4)}\end{bmatrix}\begin{bmatrix}\bar{\mathbf{x}}\\ \delta\end{bmatrix}\\ &\qquad\qquad \leq \begin{bmatrix}\mathbf{0}_{2M}\\ \cos\left(\frac{\pi}{Q}\right)\mathbf{1}_{N(Q-4)}\end{bmatrix},\\ &\text{and} \quad \begin{bmatrix}-\cos\left(\frac{\pi}{Q}\right)\mathbf{1}_{2N}\\ 0\end{bmatrix} \leq \begin{bmatrix}\bar{\mathbf{x}}\\ \delta\end{bmatrix} \leq \begin{bmatrix}\cos\left(\frac{\pi}{Q}\right)\mathbf{1}_{2N}\\ \infty\end{bmatrix}. \quad (31)\end{aligned}$$

The resulting optimization is a linear programming problem for which there exist very efficient solution methods [50]. In order to solve the problem for different P_tx values, it is sufficient to scale the solution of (31) by $\frac{P_\mathrm{tx}}{N}$ due to the linearity of the optimization.

When the optimization terminates, the optimal signal $\mathbf{x} \in \mathbb{X}^N$ is found. The signal $\mathbf{t}$ that goes through the channel is obtained as described in (1). In other words, each entry in $\mathbf{x}$ gets mapped to the corresponding CE point depending on the circular sector in which it lies.

D. Interpretation of the Safety Margin δ for PSK Signals

The safety margin δ is a parameter that affects the receiver Signal-to-Noise Ratio (SNR) and the SER. These relationships will be given for the relaxed problem; that is the quantization is omitted and we consider the relaxed received signal $\mathbf{y}'$.

The receiver SNR at the m-th user is given by

$$\mathrm{SNR}_m = \frac{\mathrm{E}\left[\left|y'_m\right|^2\right]}{\sigma_n^2} = \mathrm{E}\left[\left|y'_m\right|^2\right], \quad (32)$$

since we assume unit-variance AWGN. The expected value can be computed by averaging over N_s transmit signals. Hence, we get

$$\mathrm{SNR}_m \geq \frac{1}{N_s}\sum_{i=1}^{N_s}\left(\frac{\delta^{(i)}}{\sin\theta}\right)^2. \quad (33)$$

Thus, we can conclude that maximizing the safety margin δ leads in turn to maximizing the lower bound of the receive SNR at each user.

Moreover, it can be proven that the SER at the m-th user is upper bounded by

$$\mathrm{SER}_m \leq 1 - \frac{1}{N_s}\sum_{i=1}^{N_s}\int_{-\frac{\delta^{(i)}}{\sin\theta}}^{\infty}\mathrm{erf}\left(\frac{\delta^{(i)}}{\cos(\theta)} + \gamma\tan(\theta)\right)\frac{1}{\sqrt{\pi}} \times \mathrm{e}^{-\gamma^2}\,\mathrm{d}\gamma, \quad (34)$$

which explains why maximizing δ minimizes the SER.

V. Problem Formulation for QAM Signaling

A. The Need for an Additional Degree of Freedom α

In this section, we assume that the input signals s_m, $m = 1, \cdots, M$, belong to the S-QAM constellation, where S is assumed to be a power of 4. The QAM symbols are drawn from the set $\mathbb{S}$ defined as

$$\mathbb{S} := \{\pm(2i-1) \pm \mathrm{j}(2i-1) : i = 1, \cdots, \log_4(S)\}. \quad (35)$$

As explained in Section III, the safety margin δ has to be maximized such that the entries of the noiseless received signal $\mathbf{y}'$ belong to the intended SRs. The SRs in turn are determined by the constellation set $\mathbb{S}$ and the safety margin δ. Hence, the safety margin δ must satisfy

$$\delta \leq 1. \quad (36)$$

Independently of the available transmit power, the entries of $\mathbf{y}'$ cannot have a distance to the decision thresholds larger than 1. Hence, the available transmit power cannot be exploited to the fullest, which is a limitation of the problem formulation.

Thanks to the receive processing $\mathbf{G}$, we can introduce an additional degree of freedom α such that the entries of the received signal $\mathbf{y}'$ do not have to belong to the SRs of the set $\mathbb{S}$ but rather to a scaled version of them. That is, the QAM constellation at each receiver is scaled by α, and thus the constraint in (36) is replaced by

$$\delta \leq \alpha, \quad (37)$$

where α has to be jointly optimized with δ. Note that maximizing δ leads in turn to maximizing α, which leads to a maximal

exploitation of the available transmit power. Thus, the entries of the signal vector $\mathbf{x}$ will get closer to the polygon corners, which decreases the variations between $\mathbf{t}$ and $\mathbf{x}$.

The factor α denotes the expansion or shrinkage factor of the constellation at the receiver side depending on the available transmit power P_{tx}. As explained in Section III, the optimization problem is formulated for the specific case, i.e. $P_{\text{tx}} = N$.

B. Scaled Symbol Region for QAM Signals

In order to describe the SRs for QAM signaling in the same coordinate system for all possible QAM constellation points, we define a new coordinate system, that is a shifted and rotated version of the original coordinate system while considering α. First, the QAM coordinate system at each receiver is shifted by o_m

$$o_m = \alpha\Big(\left(\Re\{s_m\} - \operatorname{sgn}\left(\Re\{s_m\}\right)\right) + \mathrm{j}\left(\Im\{s_m\} - \operatorname{sgn}\left(\Im\{s_m\}\right)\right)\Big). \quad (38)$$

We get the following expressions for the received and the desired signal in the new coordinate system depicted in Fig. 5

$$\begin{aligned} y'_{m_{(o_m)}} &= y'_m - o_m \\ &= \mathbf{e}_m^{\mathrm{T}}\mathbf{H}\mathbf{x} - o_m \quad (39) \\ s_{m_{(o_m)}} &= \alpha s_m - o_m \\ &= \alpha\left(\operatorname{sgn}\left(\Re\{s_m\}\right) + \mathrm{j}\operatorname{sgn}\left(\Im\{s_m\}\right)\right). \quad (40) \end{aligned}$$

Second, the intermediate coordinate system is rotated by the phase of the symbol of interest $s_{m(o_m)}$. So the received signal y'_m has the following coordinates in the shifted and rotated coordinate system

$$z_{m_R} = \frac{\Re\left\{y'_{m_{(o_m)}} s^*_{m_{(o_m)}}\right\}}{|s_{m(o_m)}|}, \quad (41)$$

and

$$z_{m_I} = \frac{\Im\left\{y'_{m_{(o_m)}} s^*_{m_{(o_m)}}\right\}}{|s_{m(o_m)}|}. \quad (42)$$

We get

$$\frac{y'_{m_{(o_m)}} s^*_{m_{(o_m)}}}{|s_{m(o_m)}|} = \mathbf{e}_m^{\mathrm{T}}\left(\hat{\mathbf{H}}\mathbf{x} - \alpha\mathbf{c}\right), \quad (43)$$

where

$$\hat{\mathbf{H}} = \frac{1}{\sqrt{2}}\operatorname{diag}\left(\operatorname{sgn}\left(\Re\{\mathbf{s}\}\right) - \mathrm{j}\operatorname{sgn}\left(\Im\{\mathbf{s}\}\right)\right)\mathbf{H}, \quad (44)$$

and

$$\mathbf{c} = \frac{1}{\sqrt{2}\alpha}\operatorname{diag}\left(\operatorname{sgn}\left(\Re[\mathbf{s}]\right) - \mathrm{j}\operatorname{sgn}\left(\Im[\mathbf{s}]\right)\right)\mathbf{o}. \quad (45)$$

Note that $c_m, \forall m$, does not depend on α as can be concluded from (38) and (45). Plugging (43) into (41) and (42), we get

$$\begin{aligned} z_{m_R} &= \mathbf{e}_m^{\mathrm{T}}\mathbf{V}\bar{\mathbf{x}} - \alpha\Re\{c_m\} \quad (46) \\ z_{m_I} &= \mathbf{e}_m^{\mathrm{T}}\mathbf{W}\bar{\mathbf{x}} - \alpha\Im\{c_m\}, \quad (47) \end{aligned}$$

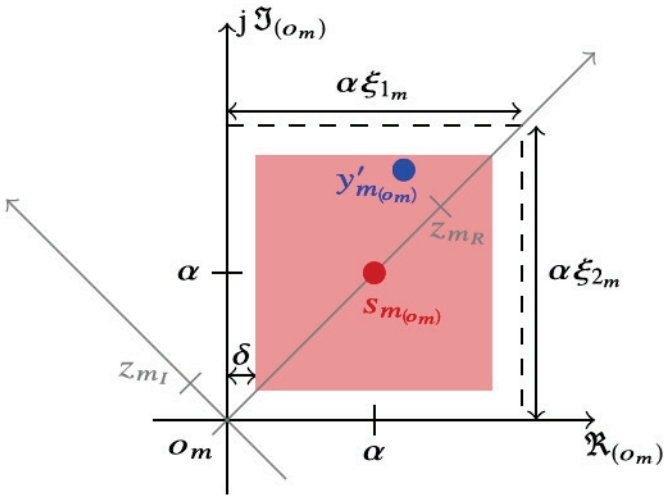

Fig. 5. Illustration of the QAM receiver symbol region for $\Re\{s_m\} > 0$ and $\Im\{s_m\} > 0$ in the shifted coordinate system (in black) and in the shifted and rotated coordinate system (in gray): $\xi_{1/2_m} \in \{2, \infty\}$.

where

$$\begin{aligned} \mathbf{V} &= \begin{bmatrix}\Re\{\hat{\mathbf{H}}\} & -\Im\{\hat{\mathbf{H}}\}\end{bmatrix} \quad (48) \\ \mathbf{W} &= \begin{bmatrix}\Im\{\hat{\mathbf{H}}\} & \Re\{\hat{\mathbf{H}}\}\end{bmatrix}. \quad (49) \end{aligned}$$

The m-th SR, as shown in Fig. 5, can hence be described by

$$\begin{aligned} z_{m_R} &\geq \sqrt{2}\delta \quad (50) \\ z_{m_R} &\leq \sqrt{\left(\alpha\xi_{1_m} - \delta\right)^2 + \left(\alpha\xi_{2_m} - \delta\right)^2} \quad (51) \\ |z_{m_I}| &\leq \left(z_{m_R} - \sqrt{2}\delta\right) \quad (52) \\ z_{m_I} &\leq -z_{m_R} + \sqrt{2}\left(\alpha\xi_{2_m} - \delta\right) \quad (53) \\ z_{m_I} &\geq z_{m_R} - \sqrt{2}\left(\alpha\xi_{1_m} - \delta\right). \quad (54) \end{aligned}$$

Note that ξ_{1_m} and $\xi_{2_m} \in \{2, \infty\}$ depending on which constellation point the symbol of interest s_m corresponds to. If s_m is one of the outer constellation points, then at least one of ξ_{1_m} or ξ_{2_m} must be equal to ∞. Since (50) and (51) are inherently fulfilled by (52), (53) and (54), the constraint of the SRs in (15) can be rewritten as

$$\begin{bmatrix} \mathbf{W}-\mathbf{V} & \mathbf{1}_M & \Re\{\mathbf{c}\} - \Im\{\mathbf{c}\} \\ -\mathbf{W}-\mathbf{V} & \mathbf{1}_M & \Re\{\mathbf{c}\} + \Im\{\mathbf{c}\} \\ \mathbf{W}+\mathbf{V} & \mathbf{1}_M & -\Re\{\mathbf{c}\} - \Im\{\mathbf{c}\} - \sqrt{2}\xi_2 \\ -\mathbf{W}+\mathbf{V} & \mathbf{1}_M & -\Re\{\mathbf{c}\} + \Im\{\mathbf{c}\} - \sqrt{2}\xi_1 \end{bmatrix} \begin{bmatrix} \bar{\mathbf{x}} \\ \sqrt{2}\delta \\ \alpha \end{bmatrix} \leq \mathbf{0}_{4M}. \quad (55)$$

C. Safety Margin δ for QAM Signals

For the QAM case, the safety margin δ in (14) can be expressed as

$$\delta = \min_m \min\Big(\frac{1}{\sqrt{2}}\left(\mathbf{z}_R - |\mathbf{z}_I|\right), \alpha\xi_1 - \frac{1}{\sqrt{2}}\left(\mathbf{z}_R - \mathbf{z}_I\right), \alpha\xi_2 - \frac{1}{\sqrt{2}}\left(\mathbf{z}_R + \mathbf{z}_I\right)\Big), \quad (56)$$

where the operator $|\bullet|$ is applied element-wise to the entries of $\mathbf{z}_I$.

$$\max_{\bar{\mathbf{x}},\delta,\alpha} \begin{bmatrix} \mathbf{0}_{2N}^{\mathrm{T}} & 1 & 0 \end{bmatrix} \begin{bmatrix} \bar{\mathbf{x}} \\ \delta \\ \alpha \end{bmatrix} \quad \text{s.t.} \quad \begin{bmatrix} \mathbf{W}-\mathbf{V} & \sqrt{2}\mathbf{1}_M & \Re\{\mathbf{c}\}-\Im\{\mathbf{c}\} \\ -\mathbf{W}-\mathbf{V} & \sqrt{2}\mathbf{1}_M & \Re\{\mathbf{c}\}+\Im\{\mathbf{c}\} \\ \mathbf{W}+\mathbf{V} & \sqrt{2}\mathbf{1}_M & -\Re\{\mathbf{c}\}-\Im\{\mathbf{c}\}-\sqrt{2}\boldsymbol{\xi}_2 \\ -\mathbf{W}+\mathbf{V} & \sqrt{2}\mathbf{1}_M & -\Re\{\mathbf{c}\}+\Im\{\mathbf{c}\}-\sqrt{2}\boldsymbol{\xi}_1 \\ \mathbf{E} & \mathbf{0}_{N(Q-4)} & \mathbf{0}_{N(Q-4)} \end{bmatrix} \begin{bmatrix} \bar{\mathbf{x}} \\ \delta \\ \alpha \end{bmatrix} \leq \begin{bmatrix} \mathbf{0}_{4M} \\ \cos\left(\frac{\pi}{Q}\right)\mathbf{1}_{N(Q-4)} \end{bmatrix}$$
$$\text{and} \quad \begin{bmatrix} -\cos\left(\frac{\pi}{Q}\right)\mathbf{1}_{2N} \\ 0 \\ 0 \end{bmatrix} \leq \begin{bmatrix} \bar{\mathbf{x}} \\ \delta \\ \alpha \end{bmatrix} \leq \begin{bmatrix} \cos\left(\frac{\pi}{Q}\right)\mathbf{1}_{2N} \\ \infty \\ \infty \end{bmatrix}. \tag{57}$$

D. Optimization Problem

We are interested in maximizing the safety margin as presented in (14). In contrast to the PSK case, there is a constraint on δ in the QAM case, stated in (37), which is inherently fulfilled by (55). Combining (14) with the SR constraint in (55) and the relaxed polygon constraint in (13), we get a linear programming problem for the design of the symbol-wise precoder for QAM signaling. The optimization problem for the case of $P_{\mathrm{tx}} = N$ is given in (57), shown at the top of this page. In order to solve the optimization problem for different P_{tx} values, it is sufficient to scale the optimal solution of (31) by $\frac{P_{\mathrm{tx}}}{N}$ due to the linearity of the optimization problem.

Again the optimized vector $\mathbf{x} \in \mathbb{X}^N$ goes through the quantizer, as stated in (1), to obtain the transmit vector $\mathbf{t}$.

E. Interpretation of the Safety Margin δ for QAM Signals

Again we consider the relaxed problem; that is the quantization is omitted and we consider the received signal $\mathbf{y}'$ instead of $\mathbf{y}$. Hence, the receive SNR at the m-th user can be approximated by

$$\mathrm{SNR}_m \approx \frac{1}{N_s}\sum_{i=1}^{N_s}(\alpha^{(i)})^2\sigma_s^2. \tag{58}$$

Since $\delta \leq \alpha$, we get

$$\mathrm{SNR}_m \geq \frac{1}{N_s}\sum_{i=1}^{N_s}(\delta^{(i)})^2\sigma_s^2. \tag{59}$$

Thus, maximizing δ results in maximizing the lower bound of the receiver SNR.

Moreover, it can be proven that the SER at the m-th user is upper bounded by

$$\mathrm{SER}_m \leq 1 + \frac{1}{N_s}\sum_{i=1}^{N_s}\int_{-z_{m,R}^{(i)}}^{2\sqrt{2}\alpha^{(i)}-z_{m,R}^{(i)}} \times \left(1-2\mathrm{erf}\left(\sqrt{2}\delta^{(i)}+\gamma\right)\right)\frac{1}{\sqrt{\pi}}\mathrm{e}^{-\gamma^2}\,\mathrm{d}\gamma. \tag{60}$$

Since erf is a monotonically increasing function, larger values of δ lead to minimize the upper bound of the SER.

F. Receive Processing

The variables of the optimization problem are the transmit vector $\mathbf{x}$, the safety margin δ and the expansion factor α. The latter determines the receive processing $\mathbf{G}$. Note that the optimal value of α is determined on a symbol-by-symbol basis, and its value cannot be communicated to the receiver. However, due to the large number of users combined with the massive MIMO assumption, the fluctuations of α across the symbols are small as explained in Section V-H. Therefore an exact value of α is not required at the receiver. Only the positions of the decision thresholds are needed to rescale the receiver constellation points to the nominal constellation points, and these only depend on the mean value of α. An estimate of the mean of α can easily be computed by averaging over a block of received signals.

After multiplication with the receiver coefficient g_m, the scaled received signal is

$$u_m = g_m r_m = g_m\,\mathrm{e}_m^{\mathrm{T}}\,\mathbf{H}\mathbf{t} + g_m\eta_m = s_m + \eta_m', \tag{61}$$

where η_m' denotes the deviation of u_m from the nominal point s_m due to the AWGN η_m, the SR constraint and the quantization applied on the relaxed optimized vector $\mathbf{x}$. Then, we can write

$$\begin{aligned} &|\Re\{r_m\}| + |\mathrm{Im}\{r_m\}| \\ &\quad = g_m^{-1}\left(|\Re\{s_m+\eta_m'\}| + |\Im\{s_m+\eta_m'\}|\right) &(62)\\ &\quad \approx g_m^{-1}\left(|\Re\{s_m\}| + |\Im\{s_m\}|\right) \\ &\qquad + g_m^{-1}\left(\Re\{\eta_m'\} + \Im\{\eta_m'\}\right), &(63)\end{aligned}$$

where the approximation is very accurate when the receiver Signal-to-Interference-Noise Ratio (SINR) is much larger than 1, which is the case for massive MIMO systems. Having zero-mean noise plus interference η_m', we get

$$\begin{aligned}\mathrm{E}[|\Re\{r_m\}| + |\Im\{r_m\}|] &\approx g_m^{-1}\mathrm{E}[|\Re\{s_m\}| + |\Im\{s_m\}|] \\ &\approx g_m^{-1}\sqrt{S}, &(64)\end{aligned}$$

when using the definition of the QAM constellation in (35). Based on (64), we propose a blind estimation method to obtain the scaling factor g_m for each user prior to the decision operation; that is

$$g_m = T \cdot \frac{\sqrt{S}}{\sum_{t=1}^{T}|\Re\{r_m[t]\}| + |\Im\{r_m[t]\}|}, \tag{65}$$

where T is the length the received sequence. The method does not require any feedback or training from the BS nor any

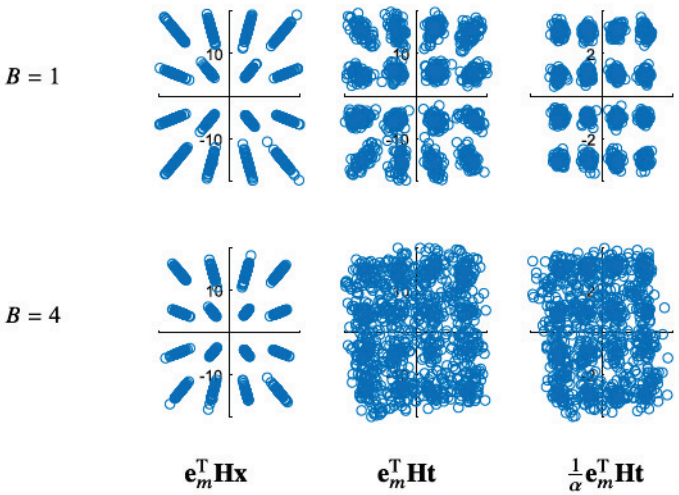

Fig. 6. The noiseless received symbols for an arbitrary user m and an arbitrary i.i.d. channel realization with $N = 64$, $M = 8$ and $Q = 4$.

knowledge of the noise plus interference power at the user terminal.

G. Symbol-Wise Processing vs. Block-Wise Processing

One might ask why we opt for symbol-wise processing and not block-wise processing. The factor α cannot be communicated to the receiver and hence has to be estimated. The estimation is based on averaging over a block of T received signals. Thus, one expects that the design of α at the transmitter has to be computed for the same block length, i.e. $B = T$. However, fixing α for a certain block length B means that B vectors $\mathbf{x}$ have to be designed jointly with a single factor α instead of having a distinct factor α for every vector $\mathbf{x}$. Additionally, the joint optimization of B vectors results in a higher-dimensional linear programming problem, where the number of inequalities is increased by a factor of B. Hence, block-wise processing not only increases the computational complexity of the problem as can be deduced from Section VI but also reduces the degrees of freedom of the optimization problem at the transmitter. This leads to the entries of the vector $\mathbf{x}$ moving farther from the polygon corners, thus increasing the quantization distortions. This effect is illustrated in Fig. 6, where the entries of $\mathbf{e}_m^{\mathrm{T}}\mathbf{H}\mathbf{x}$, $\mathbf{e}_m^{\mathrm{T}}\mathbf{H}\mathbf{t}$ and $\frac{1}{\alpha}\mathbf{e}_m^{\mathrm{T}}\mathbf{H}\mathbf{t}$ of an arbitrary user m are obtained by transmitting 1024 16-QAM signal vectors through an i.i.d. channel of coefficients $h_{mn} \sim \mathcal{CN}_{\mathbb{C}}(0,1)$, $n = 1,\cdots,N$, $m = 1,\cdots,M$, where $N = 64$, $M = 8$ and $Q = 4$. The optimization is computed for both symbol-wise processing, i.e. $B = 1$, and block-wise processing with $B = 4$. As can be deduced from the plots, block-wise processing leads to a larger safety margin with the relaxed vector $\mathbf{x}$. However, after applying the quantization this gain is lost and the symbol-wise processing is more robust against the quantization operation. This can be further explained by the results in Table I, which shows $\mathrm{E}\left[\frac{\|\mathbf{t}\neq\mathbf{x}\|_1}{N}\right]$, the percentage of entries of $\mathbf{x}$ that are distorted due to the quantization and the MSE between $\mathbf{t}$ and $\mathbf{x}$. We see that increasing B significantly increases the quantization distortion.

TABLE I
QUANTIZATION DISTORTION VS. B

	$B = 1$	$B = 4$
$\mathrm{E}\left[\frac{\|\mathbf{t}\neq\mathbf{x}\|_1}{N}\right]$	0.2176	0.4432
$\mathrm{E}\left[\|\mathbf{t}-\mathbf{x}\|_2^2\right]$	2.5458	12.6429

TABLE II
$\Delta\alpha$ AND δ_{NOM} VS. N AND M: SINGLE α

N	64		200	
M	$\Delta\alpha$	δ_{nom}	$\Delta\alpha$	δ_{nom}
2	1.3	-0.3	1.2	-0.2
8	0.5	0.2	0.4	0.3
14	0.3	0.2	0.3	0.4

TABLE III
$\Delta\alpha$ AND δ_{NOM} VS. N AND M: M α'S

N	64		200	
M	$\Delta\alpha$	δ_{nom}	$\Delta\alpha$	δ_{nom}
2	1.2	-0.2	1.1	-0.1
8	1.1	-0.8	0.5	0.3
14	1.6	-2	0.7	-0.4

Therefore, symbol-wise processing is chosen in this contribution, i.e, an optimal value of α is designed for each vector $\mathbf{x}$.

H. One Joint α vs. M Distinct α's for M Users

Symbol-wise transmit processing followed by block-wise receive processing is reliable only if the obtained values of α, i.e. $\alpha^{(i)}$, $i = 1,\cdots,T$, do not vary much from one vector $\mathbf{x}^{(i)}$ to another. Otherwise, estimating the mean value of α at the receiver would not be sufficient for correct detection. To understand this behavior, we introduce the nominal safety margin δ_{nom}, which is obtained after the receive filter $\mathbf{G}$ in the noise-free case. It can be proven that

$$\delta_{\mathrm{nom}} \geq \frac{\min_i \delta^{(i)}}{\sum_{i=1}^{T} \alpha^{(i)}/T} - 2\Delta\alpha, \tag{66}$$

where $\Delta\alpha$ represents the maximal relative fluctuation of α. From (66), we can conclude that smaller fluctuations of α lead to larger values of δ_{nom}. This observation is justified by numerical results, where the MSM optimization is run for $T = 128$ 16-QAM symbols, for 100 i.i.d. channel realizations and for $Q = 4$. The obtained values for $\Delta\alpha$ and δ_{nom} are averaged over the channels and shown in Table II and Table III. We can deduce from Table II, where a common α is designed for all users, that the values of α fluctuate less and hence δ_{nom} increases by increasing the number of users. However, no monotonic behavior of the fluctuations is noticed in Table III, which shows relatively larger values of $\Delta\alpha$ and hence smaller values of δ_{nom} compared to Table II.

VI. COMPUTATIONAL COMPLEXITY OF MSM

Both optimization problems in (31) and (57) are formulated as linear programming problems with bounded variables in

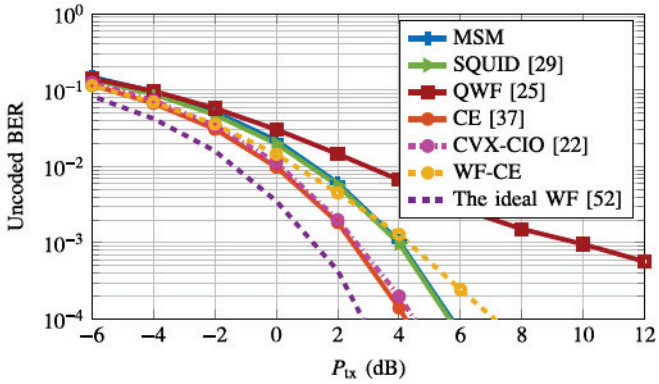

Fig. 7. Uncoded BER performance for a MU-MIMO system with $N = 64$ and $M = 8$ for different precoding designs and 4-PSK signaling.

inequality form as

$$\max_{\mathbf{x}} \mathbf{c}^{\mathrm{T}}\mathbf{x} \quad \text{s.t. } \mathbf{A}\mathbf{x} \leq \mathbf{b} \quad \text{and } \mathbf{l} \leq \mathbf{x} \leq \mathbf{u}, \tag{67}$$

where $\mathbf{c}$, $\mathbf{x}$, $\mathbf{l}$ and $\mathbf{u} \in \mathbb{R}^n$, $\mathbf{A} \in \mathbb{R}^{m \times n}$, $\mathbf{b} \in \mathbb{R}^m$ and $\mathbf{b}$ has only non-negative entries.

With the use of the simplex method to solve (67), the number of operations (multiplication and addition pairs) on each iteration is given by, [51, p. 83],

$$3m \quad \text{or} \quad (m+1)(n+1)+2m, \tag{68}$$

depending on whether pivoting is required or not. According to [51, p. 86], in most iterations no pivoting is required and hence less computation is needed.

Thus, the number of operations (multiplication and addition pairs) for each iteration for PSK and QAM signaling is on the order of

$$2N + 4MN + 8M + 2\left(Q-4\right)\left(2N^2+4N\right) \tag{69}$$

and

$$2N + 8MN + 20M + 3 + \left(Q-4\right)\left(2N^2+5N\right), \tag{70}$$

respectively. For the special case of 1-bit quantization, i.e. $Q = 4$, the complexity is linear in N and M. However, the complexity is quadratic in N for $Q > 4$. Note that the sparsity of $\mathbf{E}$ can be exploited by deploying the revised simplex method to reduce the number of required operations [51, p. 89].

VII. Simulation Results

For the simulations, we assume a BS with $N = 64$ antennas serving $M = 8$ single-antenna users. The channel $\mathbf{H}$ is composed of i.i.d. Gaussian random variables with zero-mean and unit variance. The numerical results are obtained with Monte Carlo simulations of 100 independent channel realizations. The additive noise is also i.i.d. with variance one at each antenna. The performance metric is the uncoded BER averaged over the single-antenna users. For the blind estimation of the coefficients g_m we use a block length of $T = 128$.

In the first simulation set, depicted in Fig. 7, we assume full Channel State Information (CSI), choose 4-PSK modulation and compare the uncoded BER as a function of the transmit power P_{tx} for the following precoders:

- The proposed MSM method with $Q = 4$.
- The SQUID precoder presented in [29] with $Q = 4$, where the precoder design criterion is the symbol-wise MSE between $\mathbf{u}$ and $\mathbf{s}$ under a quantization constraint. The latter is equivalent to the QCE constraint for the special case $Q = 4$. The SQUID precoder is a semi-definite relaxation based algorithm.
- The quantized Wiener Filter (WF) precoder denoted by "QWF" from [25] with $Q = 4$. This precoder design is based on linearizing the quantizer and considering the resulting quantization noise as additive Gaussian noise.
- The CE precoder presented in [37] denoted by "CE [37]", with $Q = \infty$, where the symbol-wise MSE between $\mathbf{y}$ and a scaled version of $\mathbf{s}$ is minimized under the CE constraint. The scaling factor that is applied to $\mathbf{s}$ is jointly optimized.
- The CE precoder from [22] denoted by CVX-CIO that aims at maximizing the constructive interference under the CE constraint.
- The WF precoder followed by the CE quantizer with $Q = \infty$ denoted by "WF-CE", and
- The WF precoder in the ideal case denoted by "The ideal WF" from [52], where neither quantization nor the CE constraint is applied to the transmit signal.

It can be seen that the CE constraint leads to a loss of almost 2 dB at a BER of 10^{-2} compared to the ideal WF and a loss of less than 1.5 dB when using the unquantized symbol-wise precoders proposed in [22] and [37]. The 1-bit quantization, which represents the QCE case of $Q = 4$, leads to more losses that depend on the precoder design. With the use of the linear precoder QWF a loss of more than 4 dB at a BER of 10^{-2} is noticed. However, the non-linear precoders MSM and SQUID improve the performance drastically and show a loss of slightly more than 2 dB compared to the ideal case at the cost of higher computational complexity. Nevertheless, the proposed MSM method is more efficient than SQUID as it is based on a purely linear programming formulation.

In the second simulation set, depicted in Fig. 8a and Fig. 8b, the uncoded BER is plotted as a function of the transmit power P_{tx} using the MSM precoder for different modulation schemes and two different values of Q: $Q = 4$ and $Q = 8$. Higher values of Q are omitted since the obtained results do not differ much from the case of $Q = 8$. In addition, it is beneficial in terms of computational complexity and power consumption to keep Q as small as possible. As expected, the higher the number of symbols in the modulation scheme, the higher the BER for a given P_{tx} value. However, the increase of the DAC resolution q and thus the resulting increase in Q leads to a performance improvement, which depends on the modulation scheme. Interestingly, the 16-QAM results outperform the 16-PSK results with a gain of almost 4 dB at a BER of 10^{-2} for the case of $Q = 4$, whereas in the case of $Q = 8$ the gain reduces to 3 dB and the 16-PSK modulation outperforms the 16-QAM for transmit power values larger than 15 dB.

Since the optimization problem in [22] has some similarities with our proposed MSM, we compare the uncoded

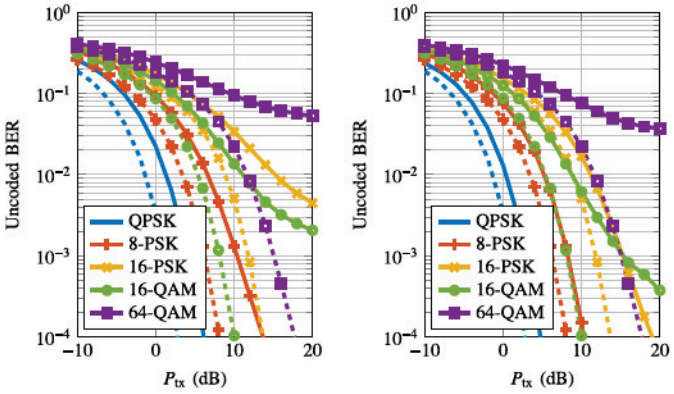

(a) $Q = 4$ (b) $Q = 8$

Fig. 8. Uncoded BER performance of MSM for a MU-MIMO system with $N = 64$ and $M = 8$ for different modulation schemes: MSM (solid lines), the ideal WF (dashed lines).

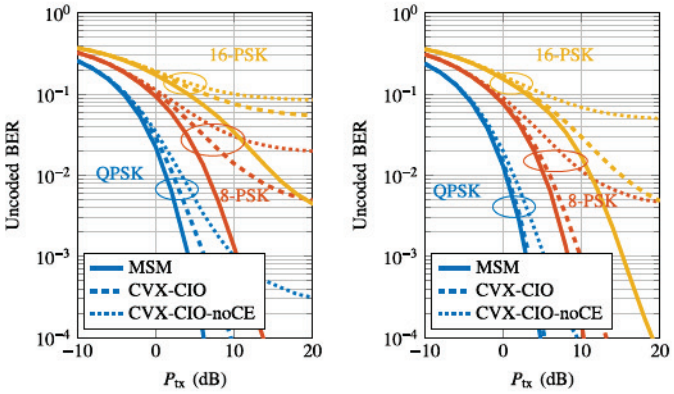

(a) $Q = 4$ (b) $Q = 8$

Fig. 9. Comparison of the uncoded BER performance between MSM, CVX-CIO from [22] and CVX-CIO-noCE for a MU-MIMO system with $N = 64$ and $M = 8$.

BER performance for both designs in Fig. 9. In our simulation, we pass the entries of x obtained by the CVX-CIO method through the CE quantizer to get QCE signals. Additionally, we introduce the method denoted by CVX-CIO-noCE that is the same as CVX-CIO with an instantaneous power constraint instead of the CE constraint. As can be seen from the results, CVX-CIO and CVX-CIO-noCE do not perform optimally under the constraint of QCE transmit signals. However, the loss compared to MSM reduces when the quantization resolution increases. The method introduced in [21], which is based on the Riemannian Conjugate Gradient (RGC) approach for CE precoding with the use of the constructive interference principle, shows similar performance as the CVX-CIO method in the quantized case.

The fourth simulation set, depicted in Fig. 10, addresses the system performance in the presence of channel estimation errors. The estimated channel is defined as

$$\mathbf{H}_\nu = \sqrt{1-\nu}\mathbf{H} + \sqrt{\nu}\mathbf{\Gamma}, \tag{71}$$

where $\mathbf{\Gamma}$ is a random matrix with i.i.d. zero-mean and unit-variance entries. We can see that the performance of the

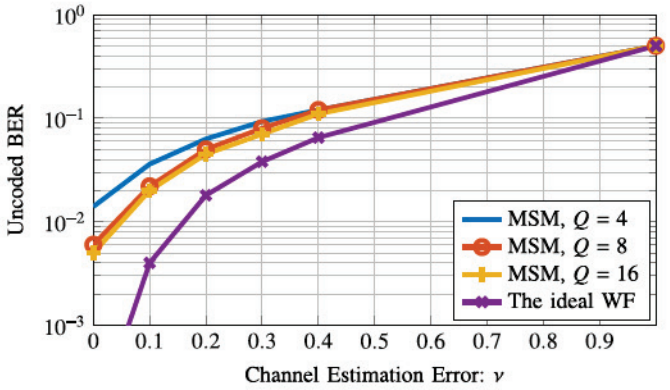

Fig. 10. Uncoded BER performance as a function of the channel estimation error variance for 16-QAM signaling and $P_{tx} = 10$ dB.

TABLE IV
AVERAGE NUMBER OF ITERATIONS OF MSM

Nb. of iter	$Q = 4$	$Q = 8$	$Q = 16$
4-PSK	45.77	121.05	187.63
8-PSK	50.15	123.91	191.55
16-PSK	54.94	128.74	199.61
16-QAM	43.25	120.42	187.32
64-QAM	43.04	120.30	188.30

proposed MSM precoder in the case of erroneous channel estimation is still better than the linear WF followed by the CE quantizer with $Q = \infty$.

In the last simulation set, we counted the average number of iterations required by the MSM precoder. The results are summarized in Table IV, where we observe that around 50 iterations are required for all modulation schemes for $Q = 4$ and more than 100 iterations for $Q > 4$.

VIII. CONCLUSION

We proposed a symbol-wise precoder for a massive MU-MIMO downlink system with coarsely QCE signals at the transmit antennas. The CE constraint is motivated by the high PA power efficiency for CE input signals, and the coarse quantization provides further power savings due to the use of the low-resolution polar DACs. The MSM precoder is based on maximizing the safety margin to the receiver decision thresholds taking the QCE constraint into account. When relaxing the QCE constraint to a linear convex set, the optimization problem can be formulated as a linear programming problem, and thus can be efficiently solved via a number of methods. The proposed precoding method comprises both PSK and QAM modulation schemes.

The extension of the proposed method to frequency-selective channels is straightforward. However, it requires higher computational complexity since block-wise processing is required to better mitigate the Inter-Symbol Interference (ISI). Our initial work on this case was presented in [35].

REFERENCES

[1] A. Osseiran *et al.*, "Scenarios for 5G mobile and wireless communications: The vision of the METIS project," *IEEE Commun. Mag.*, vol. 52, no. 5, pp. 26–35, May 2014.

[2] T. L. Marzetta, "Noncooperative cellular wireless with unlimited numbers of base station antennas," *IEEE Trans. Wireless Commun.*, vol. 9, no. 11, pp. 3590–3600, Nov. 2010.

[3] F. Rusek *et al.*, "Scaling up MIMO: Opportunities and challenges with very large arrays," *IEEE Signal Process. Mag.*, vol. 30, no. 1, pp. 40–60, Jan. 2013.

[4] J. Hoydis, S. ten Brink, and M. Debbah, "Massive MIMO in the UL/DL of cellular networks: How many antennas do we need?" *IEEE J. Sel. Areas Commun.*, vol. 31, no. 2, pp. 160–171, Feb. 2013.

[5] H. Q. Ngo, E. G. Larsson, and T. L. Marzetta, "Energy and spectral efficiency of very large multiuser MIMO systems," *IEEE Trans. Commun.*, vol. 61, no. 4, pp. 1436–1449, Apr. 2013.

[6] L. Lu, G. Y. Li, A. L. Swindlehurst, A. Ashikhmin, and R. Zhang, "An overview of massive MIMO: Benefits and challenges," *IEEE J. Sel. Topics Signal Process.*, vol. 8, no. 5, pp. 742–758, Oct. 2014.

[7] A. L. Swindlehurst, E. Ayanoglu, P. Heydari, and F. Capolino, "Millimeter-wave massive MIMO: The next wireless revolution?" *IEEE Commun. Mag.*, vol. 52, no. 9, pp. 56–62, Sep. 2014.

[8] Y. Niu, Y. Li, D. Jin, L. Su, and A. V. Vasilakos, "A survey of millimeter wave communications (mmWave) for 5G: Opportunities and challenges," *Wireless Netw.*, vol. 21, no. 8, pp. 2657–2676, 2015.

[9] T. S. Rappaport, *Millimeter Wave Wireless Communications*. Upper Saddle River NJ, USA: Prentice-Hall, 2015.

[10] *EARTH PROJECT INFSO-ICT-247733 EARTH Deliverable D2.3*, Jan. 2012.

[11] O. Blume, D. Zeller, and U. Barth, "Approaches to energy efficient wireless access networks," in *Proc. 4th Int. Symp. Commun., Control Signal Process. (ISCCSP)*, Mar. 2010, pp. 1–5.

[12] P. Varahram, S. Mohammady, B. M. Ali, and N. Sulaiman, *Power Efficiency in Broadband Wireless Communications*, 1st ed. Boca Raton, FL, USA: CRC Press, 2014.

[13] S. Cui, A. J. Goldsmith, and A. Bahai, "Energy-constrained modulation optimization," *IEEE Trans. Wireless Commun.*, vol. 4, no. 5, pp. 2349–2360, Sep. 2005.

[14] S. K. Mohammed and E. G. Larsson, "Single-user beamforming in large-scale MISO systems with per-antenna constant-envelope constraints: The doughnut channel," *IEEE Trans. Wireless Commun.*, vol. 11, no. 11, pp. 3992–4005, Nov. 2012.

[15] S. K. Mohammed and E. G. Larsson, "Per-antenna constant envelope precoding for large multi-user MIMO systems," *IEEE Trans. Commun.*, vol. 61, no. 3, pp. 1059–1071, Mar. 2013.

[16] S. K. Mohammed and E. G. Larsson, "Constant-envelope multi-user precoding for frequency-selective massive MIMO systems," *IEEE Wireless Commun. Lett.*, vol. 2, no. 5, pp. 547–550, Oct. 2013.

[17] C. Mollén and E. G. Larsson, "Multiuser MIMO precoding with per-antenna continuous-time constant-envelope constraints," in *Proc. IEEE 16th Int. Workshop Signal Process. Adv. Wireless Commun. (SPAWC)*, Jun./Jul. 2015, pp. 261–265.

[18] J.-C. Chen, "Low-complexity constant envelope precoding using finite resolution phase shifters for multiuser MIMO systems with large antenna arrays," *IEEE Trans. Veh. Technol.*, vol. 67, no. 8, pp. 7784–7789, Aug. 2018.

[19] J. Pan and W.-K. Ma, "Constant envelope precoding for single-user large-scale MISO channels: Efficient precoding and optimal designs," *IEEE J. Sel. Areas Signal Process.*, vol. 8, no. 5, pp. 982–995, Oct. 2014.

[20] S. Zhang, R. Zhang, and T. J. Lim, "MISO multicasting with constant envelope precoding," *IEEE Wireless Commun. Lett.*, vol. 5, no. 6, pp. 588–591, Dec. 2016.

[21] F. Liu, C. Masouros, P. V. Amadori, and H. Sun, "An efficient manifold algorithm for constructive interference based constant envelope precoding," *IEEE Signal Process. Lett.*, vol. 24, no. 10, pp. 1542–1546, Oct. 2017.

[22] P. V. Amadori and C. Masouros, "Constant envelope precoding by interference exploitation in phase shift keying-modulated multi-user transmission," *IEEE Trans. Wireless Commun.*, vol. 16, no. 1, pp. 538–550, Jan. 2017.

[23] H. Shen, W. Xu, A. L. Swindlehurst, and C. Zhao, "Transmitter optimization for per-antenna power constrained multi-antenna downlinks: An SLNR maximization methodology," *IEEE Trans. Signal Process.*, vol. 64, no. 10, pp. 2712–2725, May 2016.

[24] S. Zhang, R. Zhang, and T. J. Lim, "Constant envelope precoding for MIMO systems," *IEEE Trans. Commun.*, vol. 66, no. 1, pp. 149–162, Jan. 2018.

[25] A. Mezghani, R. Ghiat, and J. A. Nossek, "Transmit processing with low resolution D/A-converters," in *Proc. 16th IEEE Int. Conf. Electron., Circuits Syst. (ICECS)*, Dec. 2009, pp. 683–686.

[26] O. B. Usman, H. Jedda, A. Mezghani, and J. A. Nossek, "MMSE precoder for massive MIMO using 1-bit quantization," in *Proc. IEEE Int. Conf. Acoust., Speech Signal Process. (ICASSP)*, Mar. 2016, pp. 3381–3385.

[27] R. Price, "A useful theorem for nonlinear devices having Gaussian inputs," *IRE Trans. Inf. Theory*, vol. 4, no. 2, pp. 69–72, Jun. 1958.

[28] H. Jedda, J. A. Nossek, and A. Mezghani, "Minimum BER precoding in 1-bit massive MIMO systems," in *Proc. IEEE Sensor Array Multichannel Signal Process. Workshop (SAM)*, Jul. 2016, pp. 1–5.

[29] S. Jacobsson, G. Durisi, M. Coldrey, T. Goldstein, and C. Studer, "Nonlinear 1-bit precoding for massive MU-MIMO with higher-order modulation," in *Proc. 50th Asilomar Conf. Signals, Syst. Comput.*, Nov. 2016, pp. 763–767.

[30] S. Jacobsson, G. Durisi, M. Coldrey, T. Goldstein, and C. Studer, "Quantized precoding for massive MU-MIMO," *IEEE Trans. Commun.*, vol. 65, no. 11, pp. 4670–4684, Nov. 2017.

[31] H. Jedda, A. Mezghani, J. A. Nossek, and A. L. Swindlehurst, "Massive MIMO downlink 1-bit precoding with linear programming for PSK signaling," in *Proc. 18th IEEE Int. Workshop Signal Process. Adv. Wireless Commun. (SPAWC)*, Jul. 2017, pp. 1–5.

[32] O. Castañeda, T. Goldstein, and C. Studer, "POKEMON: A nonlinear beamforming algorithm for 1-bit massive MIMO," in *Proc. IEEE Int. Conf. Acoust., Speech Signal Process. (ICASSP)*, Mar. 2017, pp. 3464–3468.

[33] A. Swindlehurst, A. Saxena, A. Mezghani, and I. Fijalkow, "Minimum probability-of-error perturbation precoding for the one-bit massive MIMO downlink," in *Proc. IEEE Int. Conf. Acoust., Speech Signal Process. (ICASSP)*, Mar. 2017, pp. 6483–6487.

[34] O. Castañeda, S. Jacobsson, G. Durisi, M. Coldrey, T. Goldstein, and C. Studer, "1-bit massive MU-MIMO precoding in VLSI," *IEEE J. Emerg. Sel. Topics Circuits Syst.*, vol. 7, no. 4, pp. 508–522, Dec. 2017.

[35] H. Jedda, A. Mezghani, J. A. Nossek, and A. L. Swindlehurst, "Massive MIMO downlink 1-bit precoding for frequency selective channels," in *Proc. IEEE 7th Int. Workshop Comput. Adv. Multi-Sensor Adapt. Process. (CAMSAP)*, Dec. 2017, pp. 1–5.

[36] L. T. N. Landau and R. C. de Lamare, "Branch-and-bound precoding for multiuser MIMO systems with 1-bit quantization," *IEEE Wireless Commun. Lett.*, vol. 6, no. 6, pp. 770–773, Dec. 2017.

[37] A. Noll, H. Jedda, and J. A. Nossek, "PSK precoding in multi-user MISO systems," in *Proc. 21st Int. ITG Workshop Smart Antennas (WSA)*. Berlin, Germany: VDE Verlag, Mar. 2017, pp. 1–7.

[38] S. Jacobsson, O. Castañeda, C. Jeon, G. Durisi, and C. Studer, "Nonlinear precoding for phase-quantized constant-envelope massive MU-MIMO-OFDM," in *Proc. 25th Int. Conf. Telecommun. (ICT)*, Jun. 2018, pp. 367–372.

[39] A. Nedelcu *et al.*, "Quantized precoding for multi-antenna downlink channels with MAGIQ," in *Proc. 22nd Int. ITG Workshop Smart Antennas (WSA)*, Berlin, Germany: VDE Verlag, Mar. 2018, pp. 1–8.

[40] M. Kazemi, H. Aghaeinia, and T. M. Duman, "Discrete-phase constant envelope precoding for massive MIMO systems," *IEEE Trans. Commun.*, vol. 65, no. 5, pp. 2011–2021, May 2017.

[41] C. Masouros, T. Ratnarajah, M. Sellathurai, C. Papadias, and A. Shukla, "Known interference in the cellular downlink: A performance limiting factor or a source of green signal power?" *IEEE Commun. Mag.*, vol. 51, no. 10, pp. 162–171, Oct. 2013.

[42] C. Masouros and G. Zheng, "Exploiting known interference as green signal power for downlink beamforming optimization," *IEEE Trans. Signal Process.*, vol. 63, no. 14, pp. 3628–3640, Jul. 2015.

[43] H. Jedda and J. A. Nossek, "Quantized constant envelope precoding for frequency selective channels," in *Proc. IEEE Stat. Signal Process. Workshop (SSP)*, Jun. 2018, pp. 213–217.

[44] H. Jedda, M. M. Ayub, J. Munir, A. Mezghani, and J. A. Nossek, "Power- and spectral efficient communication system design using 1-bit quantization," in *Proc. Int. Symp. Wireless Commun. Syst. (ISWCS)*, Aug. 2015, pp. 296–300.

[45] H. Jedda, A. Mezghani, and J. A. Nossek, "Spectral shaping with low resolution signals," in *Proc. 49th Asilomar Conf. Signals, Syst. Comput.*, Nov. 2015, pp. 1437–1441.

[46] C. Mollén, E. G. Larsson, and T. Eriksson, "Waveforms for the massive MIMO downlink: Amplifier efficiency, distortion, and performance," *IEEE Trans. Commun.*, vol. 64, no. 12, pp. 5050–5063, Dec. 2016.

[47] Y. Li, C. Tao, A. L. Swindlehurst, A. Mezghani, and L. Liu, "Downlink achievable rate analysis in massive MIMO systems with one-bit DACs," *IEEE Commun. Lett.*, vol. 21, no. 7, pp. 1669–1672, Jul. 2017.

[48] M. T. Kabir, M. R. A. Khandaker, and C. Masouros. (2017). "Interference exploitation in full duplex communications: Trading interference power for both uplink and downlink power savings." [Online]. Available: https://arxiv.org/abs/1703.10666
[49] M. Alodeh, S. Chatzinotas, and B. Ottersten, "Symbol-level multiuser MISO precoding for multi-level adaptive modulation," *IEEE Trans. Signal Process.*, vol. 16, no. 8, pp. 5511–5524, Aug. 2017.
[50] S. P. Boyd and L. Vandenberghe, *Convex Optimization*. Cambridge, U.K.: Cambridge Univ. Press, 2004.
[51] G. B. Dantzig and M. N. Thapa, *Linear Programming* (Springer Series in Operations Research). New York, NY, USA: Springer, 1997.
[52] M. Joham, W. Utschick, and J. A. Nossek, "Linear transmit processing in MIMO communications systems," *IEEE Trans. Signal Process.*, vol. 53, no. 8, pp. 2700–2712, Aug. 2005.

Hela Jedda (S'15) received the B.S. and M.S. degrees in electrical and computer engineering from the Technical University of Munich, Germany, in 2011 and 2014, respectively, where she is currently pursuing the Ph.D. degree in information and communication engineering. In the fall term 2016, she was a Visiting Scholar with the University of California at Irvine, Irvine, CA, USA. Her research focus is on signal processing for massive multiple-input multiple-output systems with low-resolution digital-to-analog converters.

Amine Mezghani (S'08–M'16) received the Dipl.Ing. degree in electrical engineering from the Technical University of Munich, Germany, the Diplome d' Ingénieur degree from the École Centrale Paris, Paris, France, and the Ph.D. degree in electrical engineering from the Technical University of Munich in 2015. He was a Post-Doctoral Scholar with the Department of Electrical Engineering and Computer Science, University of California at Irvine, Irvine, CA, USA. In Summer 2017, he joined The University of Texas at Austin, Austin, TX, USA, as a Post-Doctoral Fellow. He has published about 100 papers, particularly on the topic of signal processing and communications with low-resolution analog-to-digital and digital-to-analog converters. His current research interests include millimeter-wave massive multiple-input multiple-output, hardware constrained radar and communication systems, and the interface between information theory and antenna theory. He was a recipient of the Joint Rohde & Schwarz and Electrical Engineering Department Outstanding Dissertation Award in 2016.

A. Lee Swindlehurst (S'83–M'84–SM'99–F'04) received the B.S. and M.S. degrees in electrical engineering from Brigham Young University (BYU) in 1985 and 1986, respectively, and the Ph.D. degree in electrical engineering from Stanford University in 1991. From 1990 to 2007, he was with the Department of Electrical and Computer Engineering, BYU, where he served as the Department Chair from 2003 to 2006. From 1996 to 1997, he held a joint appointment as a Visiting Scholar with Uppsala University and the KTH Royal Institute of Technology, Sweden. From 2006 to 2007, he was on leave working as the Vice President of Research of ArrayComm LLC, San Jose, CA, USA. Since 2007, he has been a Professor with the Electrical Engineering and Computer Science Department, University of California at Irvine, Irvine, CA, USA, where he served as the Associate Dean for Research and Graduate Studies with the Samueli School of Engineering from 2013 to 2016. From 2014 to 2017, he was a Hans Fischer Senior Fellow with the Institute for Advanced Studies, Technical University of Munich. His research focuses on array signal processing for radar, wireless communications, and biomedical applications. He has over 300 publications in these areas. He received the 2000 IEEE W. R. G. Baker Prize Paper Award, the 2006 IEEE Communications Society Stephen O. Rice Prize in the Field of Communication Theory, the 2006 and 2010 IEEE Signal Processing Society's Best Paper Awards, and the 2017 IEEE Signal Processing Society Donald G. Fink Overview Paper Award. He was the inaugural Editor-in-Chief for the IEEE JOURNAL OF SELECTED TOPICS IN SIGNAL PROCESSING.

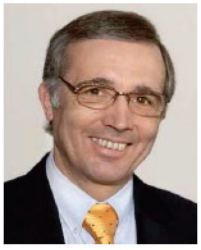

Josef A. Nossek (S'72–M'74–SM'81–F'93–LF'13) received the Dipl.Ing. and Dr.Techn. degrees in electrical engineering from the University of Technology, Vienna, Austria, in 1974 and 1980, respectively. In 1974, he joined Siemens AG. Munich, Germany, as a Member of Technical Staff, where he became a Supervisor in 1978 and has been the Head of Department of Filter Design since 1980. In 1987, he was promoted to the Head of all radio systems design. From 1989 to 2016, he was a Full Professor of circuit theory and signal processing with the Munich University of Technology (TUM). He was the President Elect, the President, and the Past President of the IEEE Circuits and Systems Society in 2001, 2002, and 2003, respectively. He was the Vice President of the Verband der Elektrotechnik, Elektronik und Informationstechnik e.V. from 2005 to 2006, the President of VDE from 2007 to 2008, and the Vice-President from 2009 to 2010. Since 2016, he has been an Emeritus of Excellence of TUM and a Full Professor with the Federal University of Ceará, Brazil. In 2009, he was an elected member of the German National Academy of Engineering Sciences (acatech). His awards include the ITG Best Paper Award in 1988, the Mannesmann Mobilfunk (now Vodafone) Innovations Award in 1998, the Award for Excellence in Teaching from the Bavarian Ministry for Science, Research and Art in 1998. He received the Golden Jubilee Medal for Outstanding Contributions to the Society in 1999 and the Education Award in 2008 from the IEEE Circuits and Systems Society. He received the Order of Merit of the Federal Republic of Germany in 2008, the Honorary Doctorate in 2013, and the Ring of Honor from VDE in 2014.